

Optical sensing of nanoparticles employing porous silicon thin films

Cite as: J. Appl. Phys. **137**, 074501 (2025); doi: [10.1063/5.0252516](https://doi.org/10.1063/5.0252516)

Submitted: 10 December 2024 · Accepted: 24 January 2025 ·

Published Online: 21 February 2025



View Online



Export Citation



CrossMark

Vered Riven,^{1,2} Chalom Zemmour,^{1,3} Tom Naor,^{1,4} Roey Sagi,^{1,4} Uri Banin,^{1,4} Micha Asscher,^{1,4} Ofra Benny,^{1,3} Jyoti Jaiswal,^{1,2,5,6,a)} and Amir Sa'ar^{1,2,a)}

AFFILIATIONS

¹The Harvey M. Kruger Family Center for Nanoscience and Nanotechnology, The Hebrew University of Jerusalem, Jerusalem, Israel

²Racah Institute of Physics, The Hebrew University of Jerusalem, Jerusalem, Israel

³Institute for Drug Research at the School of Pharmacy, The Hebrew University of Jerusalem, Jerusalem, Israel

⁴Institute of Chemistry, The Hebrew University of Jerusalem, Jerusalem, Israel

⁵Micro/Nano Technology Center, Tokai University, Kitakaname, Hiratsuka, Kanagawa 259-1292, Japan

⁶Center for Advanced Research, Dept. of Physics, Rajiv Gandhi University, Arunachal Pradesh, India

^{a)}Authors to whom correspondence should be addressed: jaiswaljyoti1988@gmail.com and saar.amir@mail.huji.ac.il

ABSTRACT

With the increasing consumption of nanomaterials in a variety of applications, our environment becomes more and more exposed to different kinds of (possibly toxic) nanomaterials having variable sizes and shapes, raising up the requirement to sense and monitor the presence of nanomaterials. Here, we propose and demonstrate a porous-silicon based optical sensing platform, capable of sensing nanoparticles of a given distribution of sizes and shapes, but independent of their chemical, mechanical, or electrical properties. A white light optical interference technique has been utilized to transduce nanoparticles trapped in the porous matrix into an optical signal. We have found an unusual optical sensing response that substantially increases the sensing bandwidth of the porous-silicon based optical sensor, which follows a Hill-equation type behavior that is characterized by a logarithmic response at low nanoparticle's concentration and saturation at high concentrations. These universal characteristics of the sensors are explained by the anomalous and limited diffusion of the nanoparticles via a quasi-1D geometry of the pore's matrix. Very low concentration of nanoparticles, of the order of few $\mu\text{g}/\text{ml}$, has been measured by this sensing technique.

01 March 2025 12:10:29

© 2025 Author(s). All article content, except where otherwise noted, is licensed under a Creative Commons Attribution-NonCommercial 4.0 International (CC BY-NC) license (<https://creativecommons.org/licenses/by-nc/4.0/>). <https://doi.org/10.1063/5.0252516>

I. INTRODUCTION

Nanotechnology in general and particularly engineered nanomaterials (e.g., synthetic nanomaterials that are produced in the lab) have attracted a great deal of attention over the recent years mainly due to the increasing number of industrial applications where nanomaterials are involved.^{1–10} Energy, aerospace, advanced materials production, electronics and displays, sensors and biosensors, drug delivery, and medical systems are just a few examples of the expanding world of applications where nanomaterials are used; see Refs. 11–17. As a result, our environment and the entire mankind become more and more exposed to nanomaterials, with the production rate steadily increasing with time,¹⁸ raising up two major questions concerning: (1) the toxicity of nanomaterials^{19–23} and (2) the impact and the damage to the environment caused by

nanomaterials.^{24–27} Thus, it is important and even urgent to develop universal capabilities to sense and monitor the presence of nanomaterials, to reduce the risk associated with exposure to nanomaterials, and to produce a cleaner environment and safer nanotechnology.

A key feature of nanotechnology is the ability to produce functional materials via controlling their shape and size down to the nanometric length scales (e.g., down to the size of a few atoms and/or molecules) and to utilize novel properties and phenomena that appear uniquely on these length scales for innovative applications.^{28–30} Therefore, sensing nanomaterials of different kinds, shapes, and sizes requires a versatile platform capable of accommodating and trapping nanomaterials with sizes ranging from a few nanometers (nm) up to hundreds of nm and even a few micrometers (μm). Very few platforms and media have such a level of versatility

and capability to act as traps for a fairly broad range of sizes. In addition, sensing requires a method to transduce capturing events (e.g., of nanoparticles) into a measurable signal, preferentially either optical or electrical.³¹ One approach is developing a sensing platform that can be considered an early warning alarm system to the presence of nanoparticles (NPs) of a given size and shape (or a range of sizes/shapes), independent of their chemical, electrical, or mechanical properties, having a wide dynamical range and a relatively fast response time. Such an early warning alarm platform for sensing might require the use of other advanced nanoscale tools for more precise analysis of the sensed NPs and their toxicity^{32,33} such as electron microscopy (SEM, TEM), nanoscale chemical analysis tools (EDX, WDS), condensation particle counters,^{34,35} or, for larger NPs (on the μm length scales), diffusion charger detectors.^{36,37}

Here, we describe a nanoparticle sensing platform that is based on a thin film of a porous matrix, capable of accommodating and trapping NPs of a given distribution of sizes and shapes, but independent of their chemical, electrical, and morphological properties. The size of the pores can be adjusted and controlled (during the fabrication stage of the porous matrix) from a few nanometers up to a few micrometers as the size of the contaminating NPs can vary over this range. However, as there are other adequate methods and technologies to sense NPs on the micrometer (or larger) length scales,^{34,38} the present work focuses on sensing of NPs having an average size less than (half) a micrometer (e.g., few nm up to few hundreds of nm) where suitable sensing platforms are still missing. This means that both the NPs and the accommodating pores are smaller than the optical wavelength of a white light source. As a result, from the point of view of the light, the porous film can be considered an effectively uniform medium having an effective refractive index (n_{eff}) that averages (in a way to be discussed later on) over the components from which, the porous medium is made of (usually, air and semiconductor/metal for the empty porous matrix). Trapping of NPs inside the porous matrix changes the effective refractive index of the porous film as a given volume fraction of the porous matrix is now occupied by NPs. Next, a sensitive optical interferometric technique, called “Refractive Interferometric Fourier Transform Spectroscopy” (RIFTS),^{39–42} has been exploited to sense variations in the effective refractive index of the porous matrix and to rapidly transduce trapping events of NPs into a measurable optical signal.

In the following, we describe the method to produce thin films of porous silicon (PSi), which has been chosen to be the material (semiconductor) from which the porous matrix is made of, due to its availability, ease of fabrication, and the versatility to adjust and tune the size of the pores (Sec. II).^{43–51} Let us point out that PSi thin films have already been used for specific binding and immobilization of NPs (such as PbS quantum dots).^{52–54} However, in most of the reports, a specific surface chemistry of the pore’s walls has been exploited to chemically bind NPs into the pores, a case that can be considered an example of a specific chemical sensing of a given type of NP, a subject that has not been investigated and discussed here. In Sec. II C, we discuss in more detail the RIFTS technique and its utilization for PSi thin films, while in Sec. III, we describe sensing experiments using three representative groups of NPs having different chemical and electrical properties. Finally, in Sec. IV we discuss the unusual universal logarithmic

sensing behavior, which was found for all three groups of NPs and has been assigned to anomalous diffusion of the NPs in the porous matrices that give rise to Hill-equation type response curve of the PSi sensors.

II. FABRICATION AND CHARACTERIZATION OF POROUS-SILICON THIN FILMS

A. Fabrication and microscopy of porous-silicon thin films

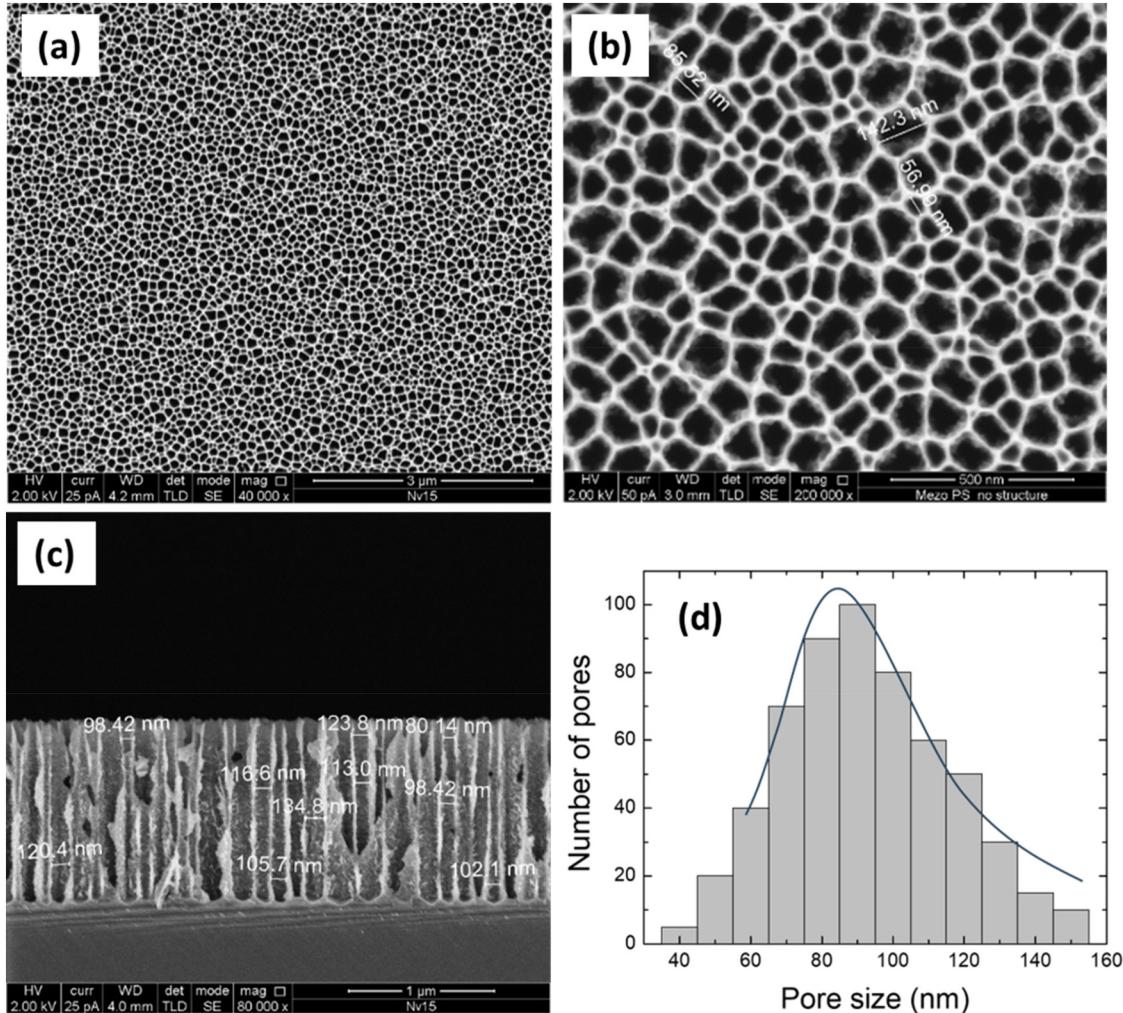
Both 100 *n*-type and *p*-type silicon wafers can be used for electrochemical etching of medium-size pores (in the range of 20 nm up to about 150–200 nm) and having a cylindrical geometry [e.g., in-plane 2D random pattern and a quasi-1D pore geometry due to a fairly uniform etching normal to the wafer plane (along the 100 direction); see Fig. 1].^{55,56} As better versatility in the pore’s widening can be achieved with *n*-type silicon wafers,⁵⁷ we have used mostly heavily doped *n*-type silicon substrates (10–20 mΩ cm, from Nova Semiconductor Inc.). An aqueous solution of hydrofluoric acid (HF, in the range of 5–9 wt. %), KMnO₄ (8 mM, as an oxidizing agent), and a surfactant (byk-348; see Ref. 58) has been used for galvanostatic etching (in the dark) at current densities in the range of 40–90 mA/cm².⁵⁷ Tuning the (average) pore’s size has mostly been accomplished via controlling the HF concentration,⁵⁷ while the current density has been adjusted to obtain relatively uniform and straight pores (e.g., minimizing the branching effect) accordingly [a method to verify this condition is by maximizing the peak-to-valley ratio of the RIFTS interference pattern (to be discussed later on)].⁵⁹ An example for a PSi film, which was electrochemically etched using 5 wt. % HF at a current density of 40 mA/cm² for 56 s, is shown in Figs. 1(a)–1(c). These SEM images have been used for measuring the pore size distribution shown in Fig. 1(d). The average pore diameter for this specific sample has been found to be $d \cong 95$ nm (with a standard deviation of $\sigma_d \cong 25$ nm).

B. Effective medium approximation

As pointed out earlier, since the pores’ size is smaller than the optical wavelength (of a white light source), one can employ effective medium models to derive an effective dielectric function (and accordingly, an effective refractive index) of the PSi medium.⁶⁰ Two popular effective medium approximations that can be utilized for PSi are the Maxwell–Garnett (MG) and the Bruggeman approximations.^{60–62} For the purpose of the current research, both models can be exploited to describe the empty (e.g., unloaded) PSi matrix, as the focus of this work, is on PSi thin films loaded with NPs. Hence, using, for example, the Bruggeman effective medium approximation (for empty PSi), we have

$$p \frac{\epsilon_M - \epsilon_{PSi}}{\epsilon_M + 2\epsilon_{PSi}} + (1-p) \frac{\epsilon_{Si} - \epsilon_{PSi}}{\epsilon_{Si} + 2\epsilon_{PSi}} = 0, \quad (1)$$

where ϵ_M is the dielectric function of the medium filling the pores (usually $\epsilon_M = \epsilon_{\text{air}} \approx 1$ for the empty pores), ϵ_{Si} is the dielectric function of silicon, ϵ_{PSi} is the effective dielectric function of the PSi medium, and p is the porosity of the medium = the volume fraction of the pores in the PSi medium. Loading now a small amount



01 March 2025 12:10:29

FIG. 1. (a)–(c) Scanning electron microscope (SEM) images of PSi thin films used in this work. (a) and (b) Top view images showing in-plane 2D random pattern of the pores. (c) Cross-sectional view image showing a quasi-1D cylindrical geometry of the pores along the 100 etching direction. (d) The corresponding pore size distribution where the average pore size is $d \cong 95 \text{ nm}$ ($\sigma_d \cong 25 \text{ nm}$).

of NPs into the pores (e.g., assuming that only a small portion of the pores' volume is occupied by NPs), one can apply a first-order perturbation theory to a second, two-component Bruggeman model [this time for the (empty) PSi + nanoparticles] to derive the following:

$$\begin{aligned} \epsilon_{\text{eff}} &\cong \epsilon_{\text{PSi}} + 2\epsilon_{\text{PSi}} \frac{\epsilon_{\text{NP}} - \epsilon_{\text{PSi}}}{\epsilon_{\text{NP}} + 2\epsilon_{\text{PSi}}} \Delta p \\ &= \frac{3\epsilon_{\text{NP}} \cdot \epsilon_{\text{PSi}}}{\epsilon_{\text{NP}} + 2\epsilon_{\text{PSi}}} \Delta p + \epsilon_{\text{PSi}}(1 - \Delta p), \end{aligned} \quad (2)$$

where ϵ_{NP} is the dielectric function of the NPs filling the pores and $\Delta p \ll p$ is the change in the porosity due to the loaded NPs. Recalling that the refractive index n_j (of the j th component of the

medium) is related to the dielectric function via $n_j = \sqrt{\epsilon_j/\epsilon_0}$ (where ϵ_j is the dielectric function of the j th component and ϵ_0 is the vacuum permittivity), we find

$$\frac{n_{\text{eff}}}{n_{\text{PSi}}} \cong 1 + \frac{n_{\text{NP}}^2 - n_{\text{PSi}}^2}{n_{\text{NP}}^2 + 2n_{\text{PSi}}^2} \Delta p. \quad (3)$$

In certain references, it has been assumed that, $n_{\text{NP}} \approx n_{\text{PSi}}$, to obtain the following linearized relationship: $n_{\text{eff}} \approx n_{\text{PSi}} + (n_{\text{NP}} - n_{\text{PSi}})\Delta p$.^{53,64} However, Eq. (3) is the more general and accurate expression and can be exploited to all kinds of NPs.

C. Reflective interferometric Fourier transform spectroscopy of PSi thin films

Figure 2(a) shows a schematic illustration of the multiple reflection process from interfaces of the PSi thin film where the incident white light (I_0) experiences reflections from the first interface (air/solution and PSi) given by an amplitude reflection coefficient, r_{12} , and a second interface (PSi/Si), given by r_{23} . The total reflection coefficient is given by⁶⁵

$$R = \frac{r_{12}^2 + r_{23}^2 + 2r_{12}r_{23}\cos(2\delta)}{1 + r_{12}^2r_{23}^2 + 2r_{12}r_{23}\cos(2\delta)}, \quad (4)$$

where

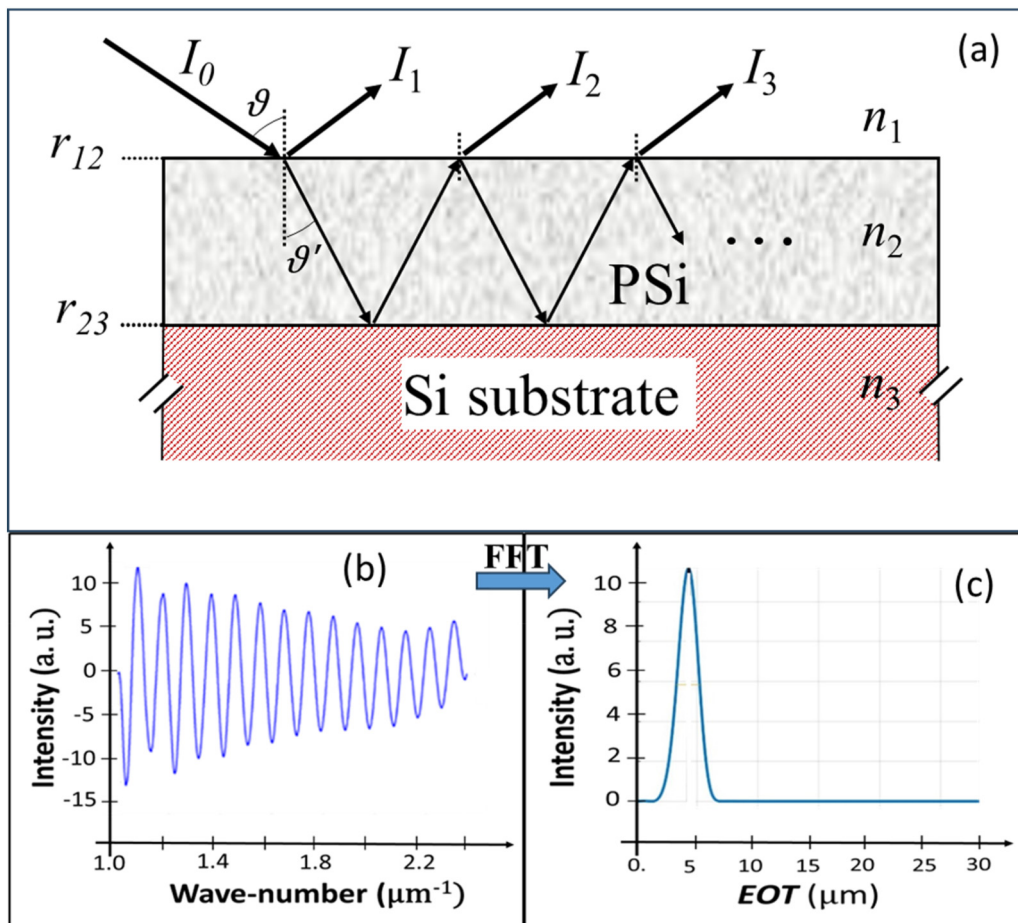
$$2\delta = 2k_0 n_{\text{eff}} L \cdot \cos \theta' = (2\pi \cdot EOT/\lambda) \cos \theta', \quad (5)$$

where 2δ is the relative phase shift between two consecutive reflected beams (for example, I_2 and I_1), θ' is the reflection angle of

the incident beam, $k_0 = 2\pi/\lambda = 2\pi\nu$ is the free space wave-vector ($\nu=1/\lambda$ is the free space wave-number and wavelength, respectively), and L is the film thickness. For normal incident reflection (e.g., $\cos \theta' = 1$) and for empty pores, $EOT = 2n_{\text{eff}}L$ becomes the effective optical thickness of the film, while the amplitude reflection coefficients take the following form:⁶⁵

$$\begin{aligned} r_{12} &= \frac{n_1 - n_2}{n_1 + n_2} = -\frac{n_{\text{eff}} - 1}{n_{\text{eff}} + 1}, \\ r_{23} &= \frac{n_2 - n_3}{n_2 + n_3} = -\frac{n_{\text{Si}} - n_{\text{eff}}}{n_{\text{Si}} + n_{\text{eff}}}. \end{aligned} \quad (6)$$

A typical reflection spectrum of the (empty) PSi film is shown in Fig. 2(b). All spectra were measured using a white light halogen lamp source (Ocean Optics HL-2000-HD) coupled to a bifurcated optical-fiber via a collimator, while the reflected beam is collected



01 March 2025 12:10:29

FIG. 2. (a) Schematic drawing of the multiple reflections and the interference from a thin film of PSi on top of the Si substrate, with r_{12} and r_{23} being the amplitude reflection coefficients for the first and the second interfaces. The total reflection is obtained by summing up all (partial) reflected beams (I_1, I_2, I_3, \dots). I_0 is the incoming beam, and n_1, n_2 , and n_3 are refractive indices of air (for the empty PSi), PSi, and Si substrate, respectively. (b) A typical reflection spectrum of PSi vs the wave-number, ν . (c) The spectrum after FFT showing a sharp peak around $4.3 \mu\text{m}$, which is the EOT of the sample.

by the fiber into the entrance port of a CCD spectrometer (Ocean Optics USB 4000). All measured spectra were normalized to a reflection from unetched, nearby area of the Si substrate. The spectrum shown in Fig. 2(b) displays a series of maxima/minima interference fringes that follow the relationship, $m\lambda_{\text{max/min}} = 2n_{\text{eff}}L = EOT$ (where m is an integer) [notice that all spectra were actually measured in the λ -space (as this is a grating spectrometer), while the measured data are displayed in the wave-number ($v = 1/\lambda$) space where maxima/minima are practically equally spaced from each other].³⁹ For the RIFTS analysis, the dc (or baseline) term has been subtracted from the spectrum to eliminate a large dc (zero-frequency) line in the fast Fourier transform (FFT) spectrum.

Next, the measured spectra were transformed into the real (x) space using a fast Fourier transform (FFT) algorithm where a Gaussian windowing function has been used to smooth the edges of the measured spectra (usually from 1 to $2.4\mu\text{m}^{-1}$). The result [for the spectrum shown in Fig. 2(b)] is presented in Fig. 2(c), showing a fairly sharp peak around, $x_{\text{max}} = EOT \approx 4.3\mu\text{m}$. Let us point out that the reflection coefficient of Eq. (4) is not a simple function of $\cos(2\delta)$ (where $2\delta = \alpha v$ and $\alpha = 2\pi \cdot EOT$). However, usually one can expand Eq. (4) in a Fourier series of $\cos(2\delta)$ where mostly the first harmonic contributes to the FFT and higher order harmonics can be ignored. Notice also that this is equivalent to practically taking only the first two reflected beams to interfere [I_1 & I_2 in Fig. 2(a)],⁶⁶ where the width of the EOT peak ($\sim 1.5\mu\text{m}$) is related to the windowing process and is mostly determined by the measurement's bandwidth. The measured, $EOT = 2n_{\text{eff}}L = (4300 \pm 100)\text{ nm}$, together with the measured thickness of the PSi film (e.g., taken from the cross-sectional SEM images of Fig. 3) $L = (900 \pm 100)\text{ nm}$, can be used to evaluate the (averaged over the visible range) effective refractive index of the (empty) PSi film,

$$n_{\text{PSi}} = EOT/2L \cong 2.4 \pm 0.2. \quad (7)$$

According to the Bruggeman approximation [Eq. (1)], this yields a porosity of about, $p = 0.45 \pm 0.05$, which is in a fairly good agreement with the porosity estimated from the SEM images of Fig. 1 and from gravimetric and dielectric measurements.^{64,67}

Finally, before moving to sensing experiments, let us relate a change in the porosity (due to the loading of NPs into the PSi matrix), Δp , to the relative change of EOT , $\Delta(EOT)/EOT$, [where $\Delta(EOT) = EOT(\Delta p) - EOT(\Delta p = 0)$]. From Eq. (3), we find

$$\Delta(EOT)/EOT(0) = \Delta n_{\text{eff}}/n_{\text{PSi}} = \frac{n_{\text{NP}}^2 - n_{\text{PSi}}^2}{n_{\text{NP}}^2 + 2n_{\text{PSi}}^2} \Delta p. \quad (8)$$

III. SENSING EXPERIMENTS

A. Groups of nanoparticles

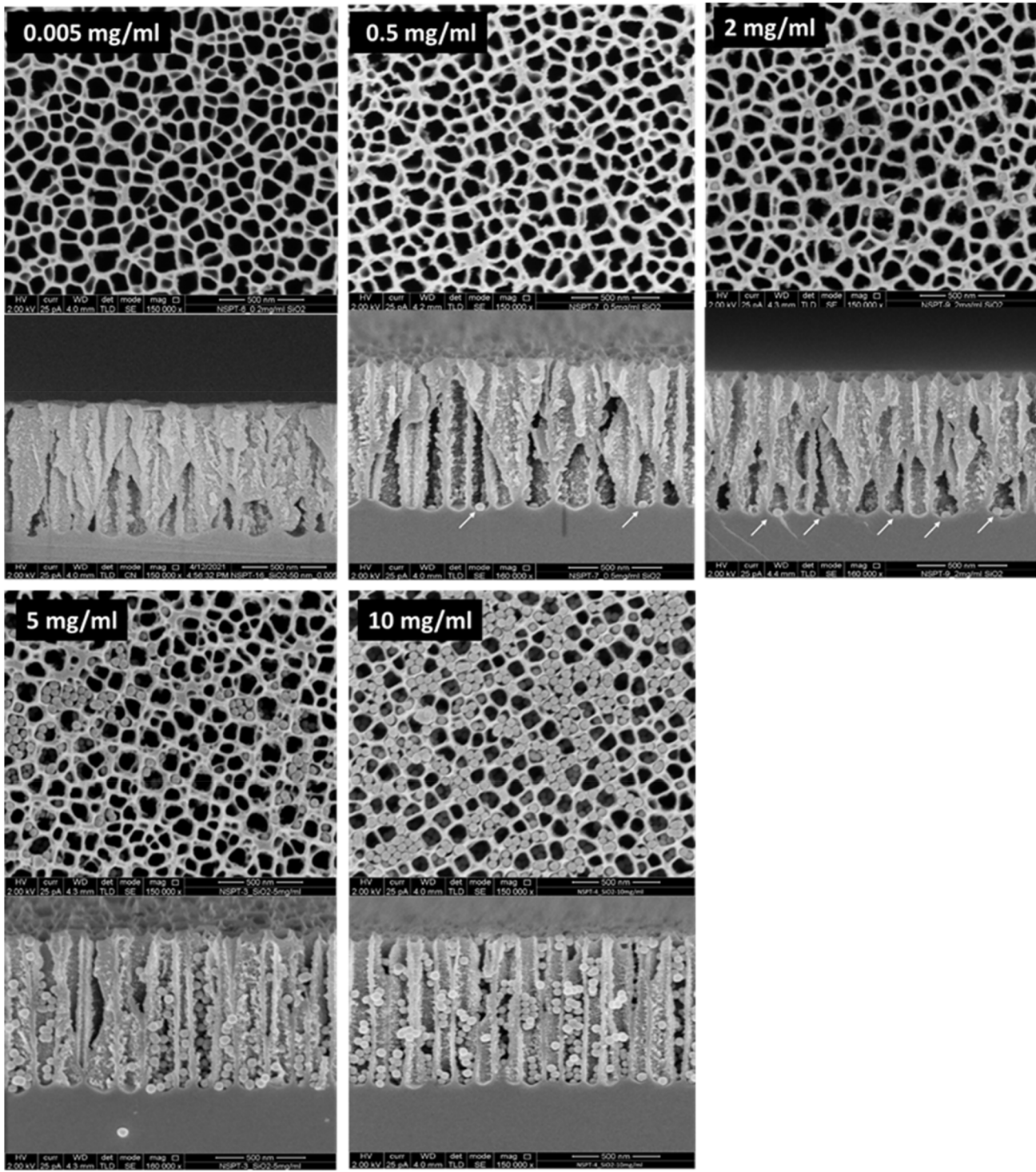
Three representative groups of NPs having different size, shape, and chemical and electrical properties have been selected for sensing experiments and include the following: (1) two sub-groups of semi-insulating silica (SiO_2) spherical NPs (S-NPs; NanoXact

silica nanospheres from nanoComposix)⁶⁸ having average diameter of (50 ± 5) and $(120 \pm 5)\text{ nm}$, respectively, (2) homemade, semiconducting ZnO nanorods (NRs) having average diameter of $(9 \pm 2)\text{ nm}$ and average length of $(35 \pm 10)\text{ nm}$ (see Refs. 69 and 70 for more details about the preparation and the properties of these NRs), and (3) homemade gold (Au) S-NPs⁷¹ (synthesized using the citrate mediated growth method; see Ref. 72) having average diameter of $(50 \pm 10)\text{ nm}$. All three groups of NPs were loaded into PSi films having an average pore diameter of $\sim 100\text{ nm}$ and size distribution like the one shown in Fig. 1(d), with a PSi thickness of about 900 nm.

B. Semi-insulating silica NPs

The following procedure has been applied to the first two sub-groups of silica NPs (having average diameter of 50 and 120 nm). At first, PSi samples underwent plasma cleaning treatment (Diener electronic, Germany; at a pressure of 6 mbar) for 1 min. Silica S-NPs were diluted in DI water to a desired concentration and introduced into a vortex mixer for 1 min followed by probe sonication for 15 s in order to minimize particle's aggregation. Next, droplets of $50\mu\text{l}$ were introduced on top of the PSi surface for 10 min to allow the diffusion of the NPs into the PSi matrix.^{51,73,74} The final stage includes spinning at 1000 rpm for 30 s followed by 3000 rpm for 1 min to remove any leftover on the PSi surface. The experiment was repeated for 12 different concentrations of NPs from 0.002 up to 10 mg/ml. Notice that the average diameter of the cylindrical pores ($\sim 95\text{ nm}$) is larger than the average diameter of the first group of silica S-NPs (50 nm), while the diameter of the second group of silica NPs (120 nm) is larger than the diameter of the pores, and, therefore, one might not expect a diffusion of these sub-groups of NPs into the pores! Spectra (in the λ -space) were measured on a time scale of few milliseconds (ms) each, which is determined essentially by the charge collection efficiency of the CCD detectors. However, in order to improve the signal-to-noise ratio (SNR), the data were digitally stored and further scans were repeated for averaging and reducing the noise, setting the scan-to-average (STA) parameter to an optimum. Typically, 200 scans with a total integration time of 1.5 s have been used for a single EOT measurement. After digitally collecting the data, FFT followed by EOT analysis and averaging over the measured EOT have been performed. Let us emphasize that the optimized noise level deduced from this STA procedure is fairly low, of the order of $\sim 0.1\text{ nm}$. Yet, as will be discussed and explained hereafter, the actual noise level of the sensing experiments is substantially larger than this value.

Figure 3 shows the pairs of top and cross-sectional SEM images of the PSi samples after sensing experiments using the 50 nm in diameter silica NPs at various concentrations. The measured $\Delta(EOT)/EOT$ for each concentration is presented by the black symbols in Fig. 4(a). Clearly, the relative change in EOT increases with the increasing concentration of (50 nm in diameter) silica NPs until a saturation is reached (above $\sim 0.03\text{ mg/ml}$). Usually, saturation represents a situation where a significant portion of the pore's volume is occupied by NPs, as, indeed, can be seen in Fig. 3 for the higher concentrations (see, e.g., 5 and 10 mg/ml in Fig. 3). As a result, the EOT signal cannot continue to increase with the



01 March 2025 12:10:29

FIG. 3. Pairs of SEM images (upper image is a top view and lower image is a cross-sectional view) of PSi films after sensing experiments using increasing concentration of 50 nm (average diameter). Silica NPs, starting from 0.005 mg/ml (upper left images) up to 10 mg/ml (lower right images). The white arrows in the mid-cross-sectional images indicate the location of silica NPs.

increasing concentration of NPs and a saturation takes place. Yet, a unique and unusual behavior has been observed for lower NP concentrations. Figure 4(b) presents a magnification of the sensor's low-concentration region down to few $\mu\text{g}/\text{ml}$ (which is the noise limit of the sensor as will be explained hereafter). It turns out that the relative change of the *EOT* decreases logarithmically with the decreasing NP concentration over about 2 orders of magnitude (notice the log-scale of the x axis in Fig. 4). This represents a highly *nonlinear* behavior of the sensing mechanism down to the

limit where the *EOT* signal is dominated by the noise. Clearly, the logarithmic behavior of the sensor is not ideal for accurate measurements of the NPs concentration. However, the logarithmic decrease of the *EOT* response allows significantly larger sensing bandwidth down to the $\mu\text{g}/\text{ml}$ concentration range [see Fig. 4(b)].

Next, a similar sensing experiment has been conducted with the 120 nm in diameter, silica S-NPs. The results of this experiment are presented by the red symbols in Fig. 4(a). Clearly, $\Delta(\text{EOT})/\text{EOT}$ is fairly low, of about 1.2×10^{-3} , and is approximately constant independent of the NP concentration. Furthermore, SEM top and cross-sectional images provide no indications of the presence of NPs in the PSi matrix (e.g., resembling the SEM images of Fig. 1). We conclude that for this size of silica NPs (120 nm), no NPs have diffused into the PSi matrix and, therefore, the measured value of $\Delta(\text{EOT})/\text{EOT}$ represents the noise level of the measurements in sensing experiments:

$$\langle \Delta(\text{EOT})/\text{EOT} \rangle_{\text{Noise}} \approx 1.2 \times 10^{-3}. \quad (9)$$

Notice that as the average *EOT* (for the empty PSi film) in our experiment is about $\langle \text{EOT} \rangle \approx 4300 \text{ nm}$, one finds $\langle \Delta(\text{EOT}) \rangle_{\text{Noise}} \approx 5 \text{ nm}$, substantially larger than the noise set by the STA procedure. We consider this estimate of the noise level to be valid for all other sensing experiments to be discussed hereafter and represent the intrinsic noise of the sensor.

C. Semiconductive ZnO nanorods

Colloidal semiconductor metal oxide ZnO NRs were synthesized by the method described in Refs. 69 and 70. To allow good dispersion in toluene, the surface of the ZnO NRs was modified by mixing 100 nmol of ZnO NRs with 50 μl of oleylamine (152 μmol) and 50 μl of 1-octanethiol (288 μmol) in 1 ml toluene, and cleaned twice with ethanol (in a 1:1 ratio of toluene to ethanol) to get rid of excess ligands. The size distribution (length and diameter) of these NRs was evaluated based on TEM images (see Refs. 69 and 70) and is shown in the insets in Figs. 6(a) and 6(b) where the average NR length is $(35 \pm 10) \text{ nm}$ (with 10 nm being the standard deviation) and the diameter is $(9 \pm 2) \text{ nm}$. NR solutions were diluted in toluene to the desired concentration, and PSi samples were plasma cleaned prior to sensing experiments. Figure 5 shows the SEM top and cross-sectional images of the PSi matrices after sensing experiments for various ZnO NR concentrations, while Fig. 6 presents the corresponding measured $\Delta(\text{EOT})/\text{EOT}$. As these colloidal NRs are fairly small (compared to all other NPs used in this work), it is not easy to locate them in SEM images due to the limited magnification. The white arrows and the yellow dashed circles in Fig. 5 were added to the images in order to assist in identifying a few of the trapped ZnO NRs.

Here again, similar sensing characteristics have been observed for the ZnO NRs with a logarithmic decrease of the sensitivity at the low-NR concentration region and a saturation at higher concentrations above $\sim 1 \text{ mg}/\text{ml}$. Notice that the red bar at the bottom of Figs. 6(a) and 6(b) represents the noise level of the measurements as deduced and set by Eq. (9). Hence, the similarity in sensing characteristics of (spherical) silica NPs and cylindrical ZnO NRs suggests that the sensing characteristics of PSi thin films are

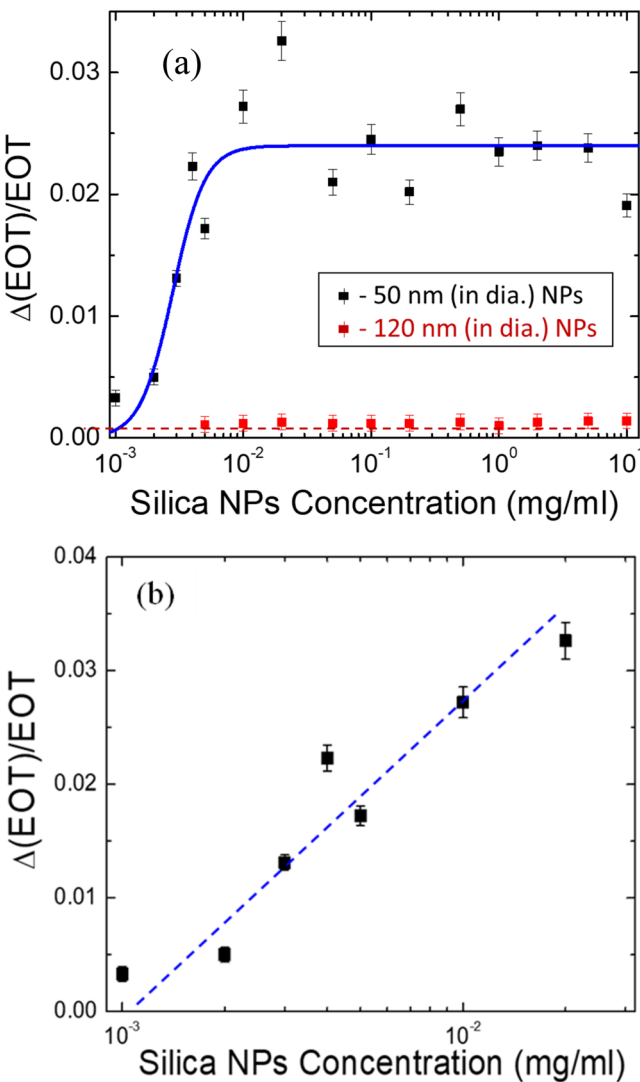
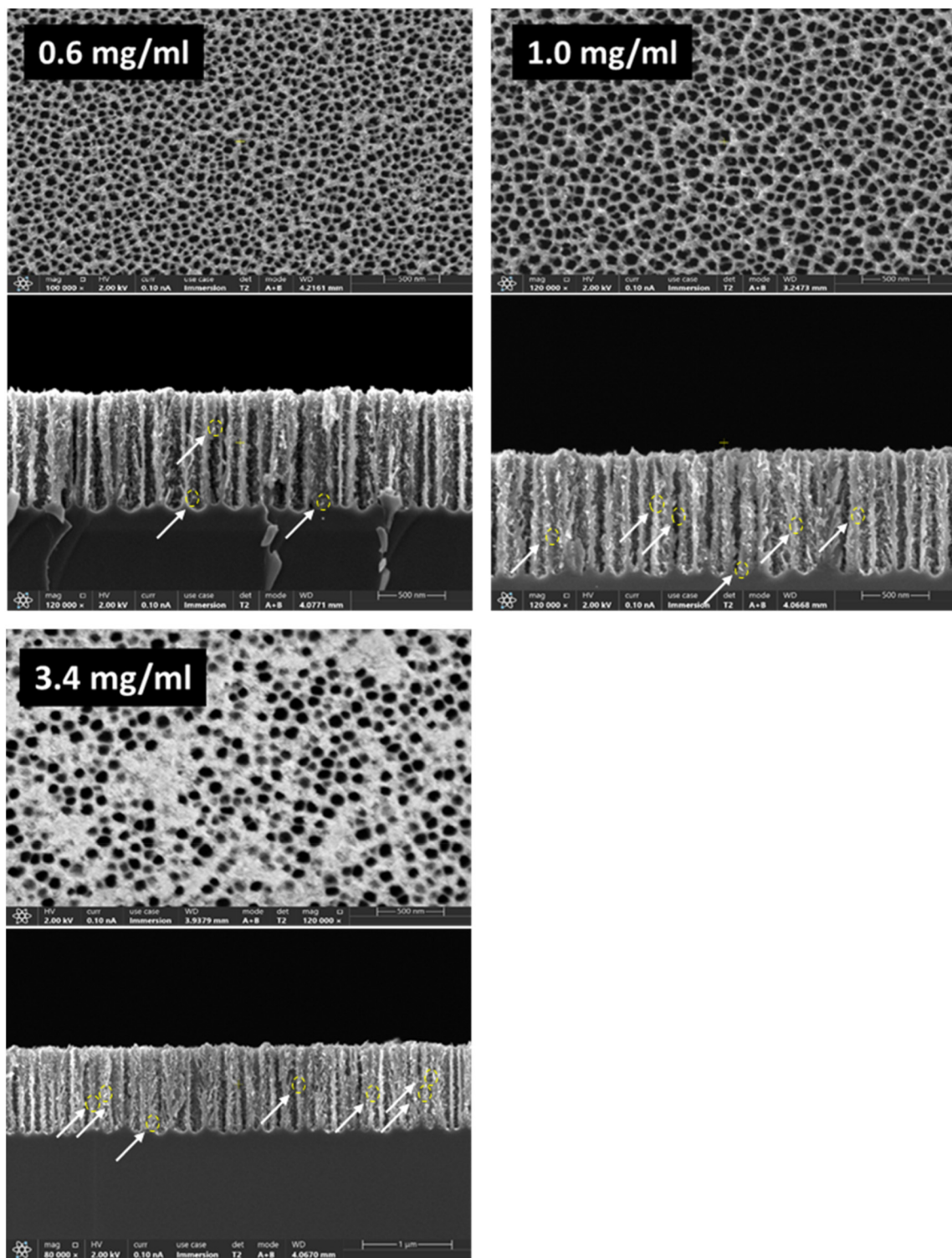


FIG. 4. The relative change in the effective optical thickness, *EOT*, vs NP concentration for 50 nm (average diameter) silica NPs (black symbols) and 120 nm silica NPs (red symbols). The solid blue line in (a) represents the best fit of the experimental data to the Hill-equation type response model given by Eq. (10). (b) Enlargement of the low-concentration region showing a logarithmic dependence on the concentration (represented by the blue dashed line).

01 March 2025 12:10:29



01 March 2025 12:10:29

FIG. 5. Pairs of SEM images (upper image is a top view and lower image is a cross-sectional view) of PSi films after sensing experiments using increasing concentration of ZnO NRs. The white arrows and the yellow dashed circles in the cross-sectional images indicate the locations of few ZnO NRs.

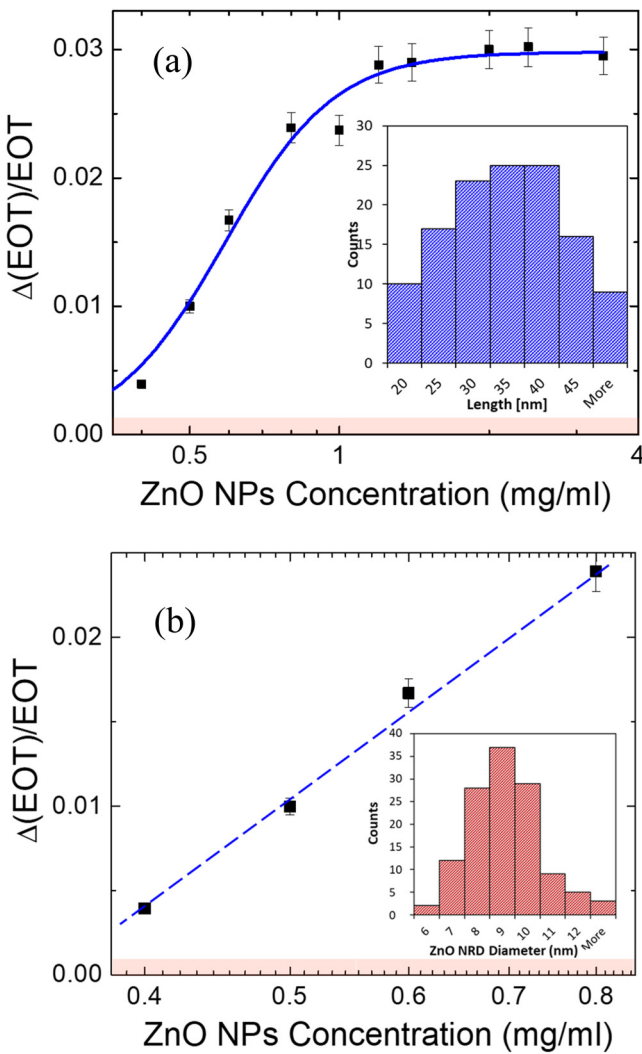


FIG. 6. (a) The relative change in EOT vs ZnO NR concentration (black symbols). The solid blue line in (a) represents the best fit to the Hill-equation type response model. (b) Enlargement of the low-concentration region to show a logarithmic dependence on the concentration (blue dashed line). The insets show size distribution of the length (a) and the diameter (b) of the ZnO NRs used in these experiments. The red bars at the bottom of both plots represent the noise level of the measurements given by Eq. (9).

universal and are independent of the specific kind, size, and shape of the sensed NPs. This hypothesis has further been tested for sensing of metallic gold (Au) spherical NPs.

D. Metallic Au NPs

HOMEMADE Au spherical NPs having an average diameter of 50 nm and a standard deviation of 10 nm have been used to test sensing of metallic NPs.⁷¹ The NPs were diluted in citrate solution to the desired concentration. Yet, we have experienced a few difficulties

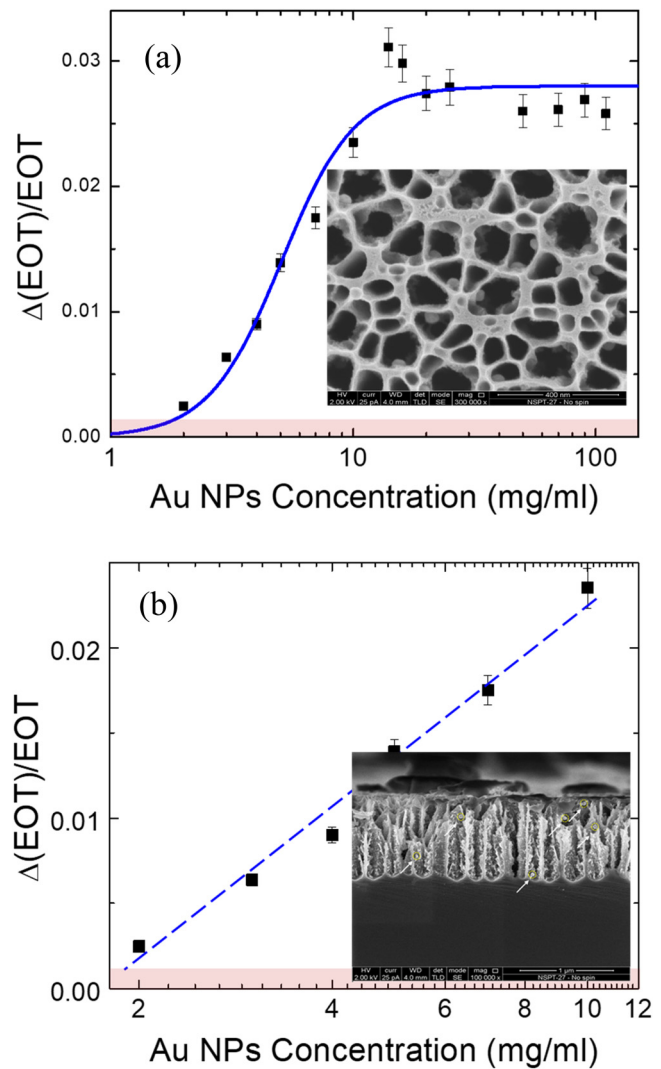


FIG. 7. The same as Fig. 6 for Au NPs with the insets showing the SEM top view (a) and cross-sectional view (b) images of PSi films after a sensing experiment at a concentration of 5 mg/ml. Here again, the white arrows and the yellow circles indicate the locations of the NPs.

in this experiment associated with the tendency of these NPs to aggregate forming macroscopically large assemblies on the PSi surface. This phenomenon degrades the optical quality of the PSi film and prohibits the diffusion of individual NPs into the PSi film. To reduce aggregation and clustering, we have coated the PSi surface with a thin layer of (3-mercaptopropyl)trimethoxysilane (MPTMS from Alfa Aesar) prior to sensing.⁷⁵ The thin MPTMS does not affect the EOT measurement of (the empty) PSi but substantially reduces the aggregation and cluster's formation. Figures 7(a) and 7(b) present the relative EOT shift vs the Au NP concentration where the insets to this figure show SEM top view [Fig. 7(a)] and cross-sectional view [Fig. 7(b)] of the PSi matrix after sensing experiment (of Au NPs) at

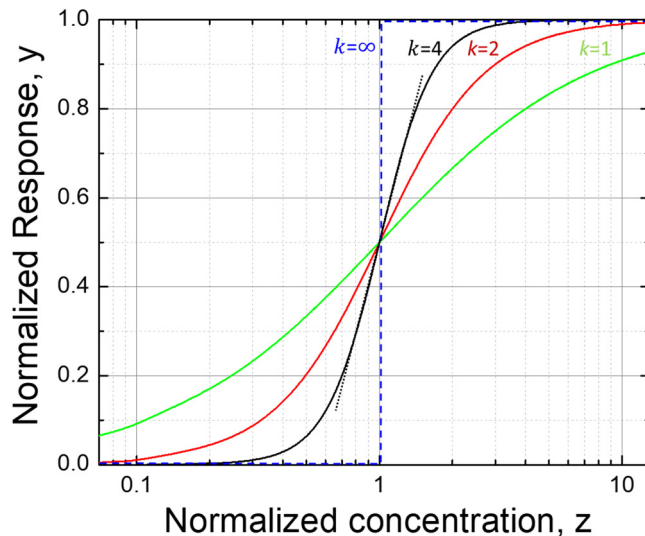


FIG. 8. Plots of the Hill-equation type response curves [Eq. (10)] for a few values of the Hill coefficient, starting with $k=1$ (green line) of the MM case, followed by $k=2$ (red line) and $k=4$ (black line). The dotted black line represents a logarithmic approximation (on semi-log scales) of the $k=4$ case, which nicely fits the Hill-equation curve over about the, $0.2 < y < 0.8$, response range. The dashed blue line represents the two-state (or stair-like) limit of $k \rightarrow \infty$.

a concentration of 5 mg/ml. Clearly, a similar behavior (to that of Silica NPs and ZnO NRs) of a saturation at high concentration and a logarithmic decrease at low-concentration region can also be observed here, with the somehow higher concentration level of NPs have been assigned to residual clustering of NPs on the PSi surface that requires higher NP concentration to obtain a saturation of $\Delta(EOT)/EOT$. Yet, the general characteristics of the sensing experiment, e.g., logarithmic behavior at low-concentration and a saturation at higher level of NPs, are still persist, thus confirming the assumption that the sensing characteristics of PSi thin films are universal.

IV. DISCUSSION

At first, let us point out that similar behavior of logarithmic response at low-concentrations followed by a saturation at higher concentrations has been found for numerous chemical and biological systems that are characterized by the Hill-equation type response function given by^{76–80}

$$y = \frac{\Delta(EOT)}{EOT} / \left[\frac{\Delta(EOT)}{EOT} \right]_{\text{Sat}} = \frac{z^k}{1+z^k}, \quad (10a)$$

with

$$z = \rho/\rho_{1/2}, \quad (10b)$$

where z is the normalized concentration, ρ is the NP concentration, and $\rho_{1/2}$ is the concentration for which the response [$\Delta(EOT)/EOT$, in the case of PSi sensors] goes down to one half (1/2) of its

saturation value, [$\langle \Delta(EOT)/EOT \rangle_{\text{Sat}}$], y is the normalized response, and k is the Hill coefficient.

The Hill-equation has traditionally been used to describe ligand-receptor reactions where the Hill coefficient, k , describes the number of ligand's binding sites on a given receptor.^{80,81} More recent and advanced interpretation relates the Hill coefficient to the level of connectivity and cooperativity among ligand binding sites,^{78,80,81} which is also affected by diffusion processes that bring the system into an equilibrium.⁷⁷ To follow the input-output relationship associated with the Hill-equation type response [Eq. (10)], we plot in Fig. 8 the Hill-equation for a few values of the Hill coefficient, k . The case of $k=1$ (e.g., the case of a single ligand's site on the receptor) is also known as the “Michaelis-Menten” (MM) equation^{82–84} and is associated with chemical enzyme-catalyzed reactions (where a given amount of chemical compound is expelled per unit time giving rise to a saturation of a rate-limited enzymatic reaction).⁸⁵ On the other hand, the Hill-equation type response having $k > 1$ represents a more complex kinetics that in the limit of a very large k ($k \gg 1$) resembles a bistable response (e.g., two-state response, as in the case of biological transistors).^{86,87} The dashed blue line in Fig. 8 represents this limit. A major feature of the Hill-equation response is the (approximately) logarithmic scaling of the middle part of the response function vs the normalized concentration where the range of logarithmic response increases with the increasing value of the Hill coefficient, k . For example, the dashed black line in Fig. 8 represents the middle range of (approximately) logarithmic response for the case of $k=4$, where the validity of the logarithmic approximation extends over the range of about $0.2 < y < 0.8$. In general, the Hill-equation response can be divided into three major regions: (1) low-concentration region where the response starts to deviate from a logarithmic behavior. Notice that for PSi NP sensors, this region usually overlaps with the noise level of the measurements [see Eq. (9)], (2) the middle-concentrations region that is characterized by a logarithmic response, and (3) a saturation region of the response at high concentrations. In addition, notice that few biological systems that are characterized by a similar Hill-equation type response have been reported to act as logarithmic sensors.^{88–90}

Moving back to the results of the sensing experiments, the solid blue lines in Fig. 4(a) (silica NPs), Fig. 6(a) (ZnO NRs), and Fig. 7(a) (Au NPs) are all represent the best fit of the experimental results to the Hill-equation type response of Eq. (10). Clearly, an excellent agreement with the experimental data has been found for all three groups of NPs, which nicely explain the logarithmic behavior presented in Figs. 4(b), 6(b), and 7(b), as well as the saturation for all three cases. In addition, the deviation from a logarithmic response at a relatively low concentration of NPs overlaps with the noise level of the measurements for all three groups of NPs [see Eq. (9)]. Fairly similar Hill coefficients have been found from the fitting procedure [of Eq. (10) to the experimental data of Figs. 4(a), 6(a), and 7(a)] for the first two groups of NPs (silica and ZnO) given by

$$k \cong 3.9 \pm 0.5, \quad (11)$$

where for the third experiment with Au NPs, somewhat lower value of k was found, ($k \cong 3.0 \pm 0.5$), a result that might be attributed to the appearance of clustering and aggregation in this experiment.

To follow a possible mechanism that might be responsible to the Hill-equation type response of PSi sensors, we point out that a basic assumption behind the MM (linear) kinetics (with $k=1$) is the presence of fast diffusion processes to retain an equilibrium between the ligands and the receptors in the reaction.^{77,84} In our case, the analogy is the equilibrium between the amount of NPs trapped in the pores and those (bulk) NPs remaining outside the pores (and do not contribute to the response of the PSi sensor). Yet, the quasi-1D cylindrical geometry of the pores and the fairly close proportion between the size of the NPs and the pores seemingly lead to anomalous and limited diffusion processes and, therefore, to a modified kinetics.^{91–93} This is particularly true for the quasi-1D geometry of the pores, which could strongly limit diffusion of NPs along the pore's axis as the connectivity between neighboring pores is quite poor.⁹⁴ Notice that in biochemical systems, similar situations of limited diffusion have been found to give rise to a breakdown of the so called, "mass action" assumption and to stochastic processes that can generate Hill-equation type response.^{77,83,91}

V. CONCLUSIONS

A method to produce an optical sensor of NPs, which is based on thin films of porous silicon, has been presented and investigated. The porous-silicon film has been designed to accommodate a given distribution of sizes and shapes of NPs, independent of their chemical or electrical properties. Transduction of NP trapping events into an optical signal is accomplished by using a sensitive interference technique (RIFTS) that detects small changes in the effective refractive index of the PSi matrix. Very low concentration of NPs, of the order of few $\mu\text{g}/\text{ml}$, has been measured by this sensing technique, which is related to a very small change in the volume of the pores ($\sim 10^{-2}$). Surprisingly, for all kinds of NPs tested in this work, we have found a Hill-equation type response that comprises a logarithmic response at low concentration of NPs and a saturation at relatively high NP concentration. This is explained by anomalous and limited diffusion of NPs into the quasi-1D matrix of pores that gives rise to a Hill-equation type kinetics. These PSi-based NP sensors can be exploited as early warning alarm sensors for the presence of contaminating NPs, thus reducing risk factors associated with overuse of nanomaterials in numerous applications of nanotechnology.

ACKNOWLEDGMENTS

This research was supported, in part (UB), by the ISRAEL SCIENCE FOUNDATION within the MAPAZ program (Grant No. 2655/23). M.A., O.B., and A.S. acknowledge the partial support by the Hebrew University "The first line of defense: selective capture of the virus" internal grant. J.J. acknowledges the Emily Erskine Endowment Postdoctoral Fund (under the Lady Davis fellowship program) for the fellowship.

AUTHOR DECLARATIONS

Conflict of Interest

The authors have no conflicts to disclose.

Author Contributions

V.R., C.Z., and T.N. contributed equally to this work.

Vered Riven: Data curation (equal); Investigation (equal); Validation (equal). **Chalom Zemmour:** Data curation (equal); Investigation (equal); Validation (equal). **Tom Naor:** Data curation (equal); Investigation (equal); Validation (equal). **Roey Sagi:** Data curation (equal); Investigation (equal); Validation (equal). **Uri Banin:** Funding acquisition (equal); Methodology (equal); Resources (equal); Supervision (equal). **Micha Asscher:** Funding acquisition (equal); Methodology (equal); Resources (equal); Supervision (equal). **Ofra Benny:** Funding acquisition (equal); Methodology (equal); Resources (equal); Supervision (equal). **Jyoti Jaiswal:** Conceptualization (equal); Data curation (equal); Formal analysis (equal); Investigation (equal); Methodology (equal); Supervision (equal). **Amir Sa'ar:** Conceptualization (equal); Funding acquisition (equal); Formal analysis (equal); Methodology (equal); Resources (equal); Supervision (equal); Writing – original draft (equal); Writing – review & editing (equal).

DATA AVAILABILITY

The data that support the findings of this study are available from the corresponding authors upon reasonable request.

REFERENCES

- ¹B. K. Teo and X. H. Sun, "Silicon-based low-dimensional nanomaterials and nanodevices," *Chem. Rev.* **107**, 1454–1532 (2007).
- ²C. Burda, X. Chen, R. Narayanan, and M. A. El-Sayed, "Chemistry and properties of nanocrystals of different shapes," *Chem. Rev.* **105**, 1025–1102 (2005).
- ³P. Alivisatos, "The use of nanocrystals in biological detection," *Nat. Biotechnol.* **22**, 47–52 (2004).
- ⁴A. Jawed, V. Saxena, and L. M. Pandey, "Engineered nanomaterials and their surface functionalization for the removal of heavy metals: A review," *J. Water Process Eng.* **33**, 101009 (2020).
- ⁵M. F. Hochella, Jr., D. W. Mogk, J. Ranville, I. C. Allen, G. W. Luther, L. C. Marr, B. P. McGrail, M. Murayama, N. P. Qafoku, K. M. Rosso, N. Sahai, P. A. Schroeder, P. Vikesland, P. Westerhoff, and Y. Yang, "Natural, incidental, and engineered nanomaterials and their impacts on the earth system," *Science* **363**, 1414 (2019). <https://www.science.org/doi/10.1126/science.aau8299>.
- ⁶M. F. Hochella, Jr. *et al.*, "Nanominerals, mineral nanoparticles, and earth systems," *Science* **319**, 1631–1635 (2008). <https://www.science.org/doi/10.1126/science.1141134>.
- ⁷F. Laborda, E. Bolea, G. Cepriá, M. T. Gómez, M. S. Jiménez, J. Pérez-Arantegui, and J. R. Castillo, "Detection, characterization and quantification of inorganic engineered nanomaterials: A review of techniques and methodological approaches for the analysis of complex samples," *Anal. Chim. Acta* **904**, 10–32 (2016).
- ⁸K. Sobolev and M. F. Gutierrez, "How nanotechnology can change the concrete world," *Am. Ceram. Soc. Bull.* **84**, 16–20 (2005). <https://bpb-us-w2.wpmucdn.com/sites.uwm.edu/dist/f/324/files/2016/10/SobolevP2-p3teoe.pdf>.
- ⁹K. Havancsák, "Nanotechnology at present and its promise for the future," *Mater. Sci. Forum* **414–415**, 85–94 (2003).
- ¹⁰"Industrial applications of nanomaterials," in *Micro and Nano Technologies*, edited by S. Thomas, Y. Grohens, and Y. B. Pottathara (Elsevier, Amsterdam, 2019). <https://www.sciencedirect.com/book/9780128157497/industrial-applications-of-nanomaterials#book-info>.

- ¹¹J. L. West and N. J. Halas, "Engineered nanomaterials for biophotonics applications: Improving sensing, imaging, and therapeutics," *Annu. Rev. Biomed. Eng.* **5**, 285–292 (2003).
- ¹²A. A. Keller and A. Lazareva, "Predicted releases of engineered nanomaterials: From global to regional to local," *Environ. Sci. Technol. Lett.* **1**, 65–70 (2014).
- ¹³S. Syama and P. V. Mohanan, "The promising biomedical applications of engineered nanomaterial," in *Handbook of Nanomaterials for Industrial Applications*, edited by C. M. Hussain (Elsevier, 2018), Chap. 29, pp. 530–542.
- ¹⁴T. Arfin and A. Tarannum, "Engineered nanomaterials for industrial application: An overview," in *Handbook of Nanomaterials for Industrial Applications*, edited by C. M. Hussain (Elsevier, 2018), Chap. 6, pp. 127–134.
- ¹⁵S. D'Mello, C. Cruz, M. L. Chen *et al.*, "The evolving landscape of drug products containing nanomaterials in the United States," *Nat. Nanotech.* **12**, 523–529 (2017).
- ¹⁶J. Pulit-Prociak and M. Banach, "Silver nanoparticles—A material of the future?," *Open Chem.* **14**, 76–91 (2016).
- ¹⁷Y. E. Panfil, M. Oded, and U. Banin, "Colloidal quantum nanostructures: Emerging materials for display applications," *Chem. Eng. J.* **57**, 4274–4295 (2018).
- ¹⁸See <https://www.grandviewresearch.com/industry-analysis/nanotechnology-and-nanomaterials-market#> for information about "Nanomaterials Market Size, Growth Rate | Report, 2023–2030" (grand view research, Report ID: GVR-4-68038-565-6).
- ¹⁹S. Sharifi, S. Behzadi, S. Laurent, M. Laird Forrest, P. Stroeve, and M. Mahmoudi, "Toxicity of nanomaterials," *Chem. Soc. Rev.* **41**, 2323 (2012).
- ²⁰G. V. Vimbela, S. M. Ngo, C. Fraze, L. Yang, and D. A. Stout, "Antibacterial properties and toxicity from metallic nanomaterials," *Int. J. Nanomed.* **12**, 3941–3965 (2017).
- ²¹X. Yuan, X. Zhang, L. Sun *et al.*, "Cellular toxicity and immunological effects of carbon-based nanomaterials," *Part. Fibre Toxicol.* **16**, 18 (2019).
- ²²Z. Peng, X. Liu, W. Zhang *et al.*, "Advances in the application, toxicity and degradation of carbon nanomaterials in environment: A review," *Environ. Int.* **134**, 105298 (2020).
- ²³P. C. Ray, H. Yu, and P. P. Fu, "Toxicity and environmental risks of nanomaterials: Challenges and future needs," *J. Environ. Sci. Health C* **27**, 1–35 (2009).
- ²⁴J. R. Lead, G. E. Batley, P. J. Alvarez, M. N. Croteau, R. D. Handy, M. J. McLaughlin, J. D. Judy, K. Schirmer, "Nanomaterials in the environment behavior, fate, bioavailability, and effects—An updated review," *Environ. Toxicol. Chem.* **37**, 2029–2063 (2018).
- ²⁵K. L. Garner, S. Suh, and A. A. Keller, "Assessing the risk of engineered nanomaterials in the environment: Development and application of the nanoFate model," *Environ. Sci. Technol.* **51**, 5541–5551 (2017).
- ²⁶M. N. Khan, M. Mobin, Z. K. Abbas, K. A. AlMutairi, and Z. H. Siddiqui, "Role of nanomaterials in plants under challenging environments," *Plant Physiol. Biochem.* **110**, 194–209 (2017).
- ²⁷G. V. Lowry, K. B. Gregory, S. C. Apte, and J. R. Lead, "Transformations of nanomaterials in the environment," *Environ. Sci. Technol.* **46**, 6893–6899 (2012).
- ²⁸R. Valiev, "Materials science: Nanomaterial advantage," *Nature* **419**, 887–889 (2002).
- ²⁹I. A. Ovid'ko, R. Z. Valiev, and Y. T. Zhu, "Review on superior strength and enhanced ductility of metallic nanomaterials," *Prog. Mater. Sci.* **94**, 462–540 (2018).
- ³⁰D. Guo, G. Xie, and J. Luo, "Mechanical properties of nanoparticles: Basics and applications," *J. Phys. D: Appl. Phys.* **47**, 013001 (2014).
- ³¹In *Handbook of Optical Sensors*, edited by J. L. Santos, and F. Farahi (CRC Press, Boca Raton, FL, 2014).
- ³²T. A. J. Kuhlbusch, S. W. P. Wijnhoven, and A. Haase, "Nanomaterial exposures for worker, consumer and the general public," *NanoImpact* **10**, 11–25 (2018).
- ³³C. Asbach, H. Fissan, B. Stahlmecke, T. A. J. Kuhlbusch, and D. Y. H. Pui, "Conceptual limitations and extensions of lung-deposited nanoparticle surface area monitor (NSAM)," *J. Nanopart. Res.* **11**, 101–109 (2009).
- ³⁴S. V. Hering, M. R. Stolzenburg, F. R. Quant, D. R. Oberreit, and P. B. Keady, "A laminar-flow, water-based condensation particle counter (WCPC)," *Aerosol Sci. Technol.* **39**, 659–672 (2005).
- ³⁵T. A. J. Kuhlbusch, C. Asbach, H. Fissan, D. Göhler, and M. Stintz, "Nanoparticle exposure at nanotechnology workplaces: A review," *Part. Fibre Toxicol.* **8**, 22 (2011).
- ³⁶G. Biskos, K. Reavell, and N. Collings, "Unipolar diffusion charging of aerosol particles in the transition regime," *J. Aerosol Sci.* **36**, 247–265 (2005).
- ³⁷H. Kaminski, T. A. J. Kuhlbusch, S. Rath, U. Götz, M. Sprenger, D. Wels, J. Pollock, V. Bachmann, N. Dziurowitz, H. J. Kiesling, A. Schwiegelshohn, C. Monz, D. Dahmann, and C. Asbach, "Comparability of mobility particle sizers and diffusion chargers," *J. Aerosol Sci.* **57**, 156–178 (2013).
- ³⁸Y. Mirsky, A. Nahor, E. Edrei, N. Massad-Ivanir, L. M. Bonanno, E. Segal, and A. Sa'ar, "Optical biosensing of bacteria and cells using porous silicon based, photonic lamellar gratings," *Appl. Phys. Lett.* **103**, 033702 (2013).
- ³⁹C. Pacholski, M. Sartor, M. J. Sailor, F. Cunin, and G. M. Miskelly, "Biosensing using porous silicon double-layer interferometers: Reflective interferometric Fourier transform spectroscopy," *J. Am. Chem. Soc.* **127**, 11636–11645 (2005).
- ⁴⁰C. Pacholski, C. Yu, G. M. Miskelly, D. Godin, and M. J. Sailor, "Reflective interferometric Fourier transform spectroscopy: A self-compensating label-free immunosensor using double-layers of porous SiO₂," *J. Am. Chem. Soc.* **128**, 4250–4252 (2006).
- ⁴¹C. Pacholski, L. Perelman, M. S. VanNieuwenhze, and M. J. Sailor, "Small molecule detection by reflective interferometric Fourier transform spectroscopy (RIFTS)," *Phys. Status Solidi A* **206**, 1318–1321 (2009).
- ⁴²M. P. Schwartz, S. D. Alvarez, and M. J. Sailor, "Porous SiO₂ interferometric biosensor for quantitative determination of protein interactions: Binding of protein A to immunoglobulins derived from different species," *Anal. Chem.* **79**, 327–334 (2007).
- ⁴³H. Föll, M. Christoffersen, J. Carstensen, and G. Hasse, "Formation and application of porous silicon," *Mater. Sci. Eng., R* **39**, 93–141 (2002).
- ⁴⁴P. Granitzer and K. Rumpf, "Porous silicon-A versatile host material," *Materials* **3**, 943–998 (2010).
- ⁴⁵F. A. Harraz, "Porous silicon chemical sensors and biosensors: A review," *Sens. Actuators, B* **202**, 897–912 (2014).
- ⁴⁶I. Ivanov, V. Skryshevsky, and A. Belarouci, "Engineering porous silicon-based microcavity for chemical sensing," *ACS Omega* **8**, 21265–21276 (2023).
- ⁴⁷E. Moghimi and M. E. Azim Araghi, "Ethanol and acetone gas sensor properties of porous silicon based on resistance response," *Silicon* **15**, 5821–5827 (2023).
- ⁴⁸V. Torres-Costa and R. J. Martín-Palma, "Application of nanostructured porous silicon in the field of optics. A review," *J. Mater. Sci.* **45**, 2823–2838 (2010).
- ⁴⁹G. Ayvazyan, K. Ayvazyan, L. Hakhoyan, and A. Semchenko, "NO₂ gas sensor based on pristine black silicon formed by reactive Ion etching," *Phys. Status Solidi RRL* **17**, 2300058 (2023).
- ⁵⁰B. Urbach, E. Axelrod, and A. Sa'ar, "Correlation between transport, dielectric and optical properties of oxidized and non-oxidized porous silicon," *Phys. Rev. B* **75**, 205330 (2007).
- ⁵¹N. Arad-Vosk, A. Yakov, and A. Sa'ar, "Size, porosity and surface-termination dependence of the radiative and nonradiative relaxation processes of porous silicon," *J. Appl. Phys.* **127**, 164304 (2020).
- ⁵²G. Gaur, D. S. Koktysh, and S. M. Weiss, "Immobilization of quantum dots in nanostructured porous silicon films: Characterizations and signal amplification for dual-mode optical biosensing," *Adv. Funct. Mater.* **23**, 3604–3614 (2013).
- ⁵³G. Gaur, D. S. Koktysh, D. M. Fleetwood, R. A. Weller, R. A. Reed, and S. M. Weiss, "Influence of interfacial oxide on the optical properties of single layer CdTe/CdS quantum dots in porous silicon scaffolds," *Appl. Phys. Lett.* **107**, 063106–063111 (2015).
- ⁵⁴G. Mula, T. Printemps, C. Licita *et al.*, "Doping porous silicon with erbium: Pores filling as a method to limit the Er-clustering effects and increasing its light emission," *Sci. Rep.* **7**, 5957 (2017).

- ⁵⁵V. Lehmann, *Electrochemistry of Silicon* (Wiley-VCH Verlag, GmbH, Weinheim, 2002). <https://onlinelibrary.wiley.com/doi/book/10.1002/3527600272>.
- ⁵⁶A. Nahor, O. Berger, Y. Bardavid, G. Toker, Y. Tamar, L. Reiss, M. Asscher, S. Yitzchaik, and A. Sa'ar, "Hybrid structures of porous silicon and conjugated polymers for photovoltaic applications," *Phys. Status Solidi C* **8**, 1908–1912 (2011).
- ⁵⁷Y. H. Ogata, A. Koyama, F. A. Harraz, M. S. Salem, and T. Sakka, "Electrochemical formation of porous silicon with medium-sized pores," *Electrochemistry* **75**, 270 (2007).
- ⁵⁸See <https://www.byk.com/en/products/additives-by-name/byk-348> for information about BYK-348, the silicon surfactant used in our experiments.
- ⁵⁹H. Ouyang, M. Christoffersen, R. Viard, B. L. Miller, and P. M. Fauchet, "Macroporous silicon microcavities for macromolecule detection," *Adv. Funct. Mater.* **15**, 1851–1859 (2005).
- ⁶⁰W. Theiß, "Optical properties of porous silicon," *Surf. Sci. Rep.* **29**, 91–192 (1997).
- ⁶¹W. Theiß, S. Henkel, and M. Arntzen, "Connecting microscopic and macroscopic properties of porous media: Choosing appropriate effective medium concepts," *Thin Solid Films* **255**, 177–180 (1995).
- ⁶²J. Sancho-Parramon, V. Janicki, and H. Zorc, "On the dielectric function tuning of random metal-dielectric nanocomposites for metamaterial applications," *Opt. Express* **18**, 26915 (2010).
- ⁶³C. Lee, L. Koker, and K. W. Kolasinski, "A novel optical technique for the estimation of porosity in porous silicon thin films," *Appl. Phys. A* **71**, 77–82 (2000).
- ⁶⁴M. J. Sailor, *Porous Silicon in Practice: Preparation, Characterization and Applications* (Wiley-VCH, Weinheim, 2012). <https://onlinelibrary.wiley.com/doi/book/10.1002/9783527641901>.
- ⁶⁵M. Born, E. Wolf, A. B. Bhatia, P. C. Clemmow, D. Gabor, A. R. Stokes, A. M. Taylor, P. A. Wayman, and W. L. Wilcock, *Principles of Optics*, 7th ed. (Cambridge University Press, Cambridge, 1999), pp. 65.
- ⁶⁶G. Kraus, A. Brecht, V. Vasic, and G. Gauglitz, "Polymer based RIFS sensing: An approach to the indirect measurement of organic pollutants in water," *Fresenius J. Anal. Chem.* **344**, 598–601 (1994).
- ⁶⁷E. Axelrod, A. Givant, J. Shappir, Y. Feldman, and A. Sa'ar, "Dielectric relaxation and porosity determination of porous silicon," *J. Non-Cryst. Solids* **305**, 235–242 (2002).
- ⁶⁸See <https://nanocomposix.com/> for information about silica NPs from nanoComposix.
- ⁶⁹A. Pinkas, N. Waiskopf, S. Gigi, T. Naor, A. Layani, and U. Banin, "Morphology effect on zinc oxide quantum photoinitiators for radical polymerization," *Nanoscale* **13**, 7152–7160 (2021).
- ⁷⁰T. Naor, S. Gigi, N. Waiskopf, G. Jacobi, S. Shoshani, D. Kam, S. Magdassi, E. Banin, and U. Banin, "ZnO quantum photoinitiators as an all-in-one solution for multifunctional photopolymer nanocomposites," *ACS Nano* **17**, 20366–20375 (2023).
- ⁷¹N. Friedman, A. Dagan, J. Elia, S. Merims, and O. Benny, "Physical properties of gold nanoparticles affect skin penetration via hair follicles," *Nanomedicine* **36**, 102414 (2021).
- ⁷²N. G. Bastús, J. Comenge, and V. Puntes, "Kinetically controlled seeded growth synthesis of citrate-stabilized gold nanoparticles of up to 200 nm: Size focusing versus Ostwald ripening," *Langmuir* **27**, 11098–11105 (2011).
- ⁷³B. Urbach, N. Korbakov, Y. Bar-David, S. Yitzchaik, and A. Sa'ar, "Composite structures of polyaniline and meso porous silicon: Electrochemistry, optical and transport properties," *J. Phys. Chem. C* **111**, 16586–16592 (2007).
- ⁷⁴N. Arad-Vosk and A. Sa'ar, "Radiative and nonradiative relaxation phenomena in hydrogen- and oxygen- terminated porous silicon," *Nanoscale Res. Lett.* **9**, 47 (2014).
- ⁷⁵J.-R. Li, K. L. Lusker, J.-J. Yu, and J. C. Garno, "Engineering the spatial selectivity of surfaces at the nanoscale using particle lithography combined with vapor deposition of organosilanes," *ACS Nano* **3**, 2023–2035 (2009).
- ⁷⁶J. N. Weiss, "The Hill equation revisited: Uses and misuses," *FASEB J.* **11**, 835–841 (1997).
- ⁷⁷S. A. Frank, "Input-output relations in biological systems: Measurement, information and the Hill equation," *Biol. Direct* **8**, 31 (2013).
- ⁷⁸Q. Zhang, S. Bhattacharya, and M. E. Andersen, "Ultrasensitive response motifs: Basic amplifiers in molecular signaling networks," *Open Biol.* **3**, 130031–130010 (2013).
- ⁷⁹S. Bottani and R. A. Veitia, "Hill function-based models of transcriptional switches: Impact of specific, nonspecific, functional and nonfunctional binding," *Biol. Rev.* **92**, 953–996 (2017).
- ⁸⁰M. Santillán, "On the use of the Hill functions in mathematical models of gene regulatory networks," *Math. Model. Nat. Phenom.* **3**, 85–97 (2008).
- ⁸¹R. Gesztelyi, J. Zsuga, A. Kemeny-Beke *et al.*, "The Hill equation and the origin of quantitative pharmacology," *Arch. Hist. Exact Sci.* **66**, 427–438 (2012).
- ⁸²P. Atkins and J. de Paula, *Physical Chemistry*, 7th ed. (Oxford University Press, Oxford, NY, 2002), pp. 910. <https://global.oup.com/ukhe/product/atkins-physical-chemistry-9780198847816?cc=il&lang=en&c>.
- ⁸³M. A. Savageau, "Michaelis-Menten mechanism reconsidered: Implications of fractal kinetics," *J. Theor. Biol.* **176**, 115–124 (1995).
- ⁸⁴S. Schnell, "Validity of the Michaelis-Menten equation—Steady-state or reactant stationary assumption: That is the question," *FEBS J.* **281**, 464–472 (2014).
- ⁸⁵A. Cornish-Bowden, *Fundamentals of Enzyme Kinetics* (Wiley-Blackwell, Hoboken, NJ, 2012). <https://www.wiley.com/en-ae/Fundamentals+of+Enzyme+Kinetics,+4th+Edition-p-9783527330744>.
- ⁸⁶R. Sarapeshkar, *Ultra Low Power Bioelectronics: Fundamentals, Biomedical Applications, and Bio-Inspired Systems* (Cambridge University Press, Cambridge, 2010).
- ⁸⁷M. D. Leach, E. Klipp, L. E. Cowen, and J. P. Brown, "Fungal Hsp90: A biological transistor that tunes cellular outputs to thermal inputs," *Nat. Rev. Microbiol.* **10**, 693–704 (2012).
- ⁸⁸S. A. Frank, "A biochemical logarithmic sensor with broad dynamic range [version 3; peer review: 2 approved]," *FI1000Research* **7**, 200 (2018).
- ⁸⁹R. Daniel, J. R. Rubens, R. Sarapeshkar *et al.*, "Synthetic analog computation in living cells," *Nature* **497**, 619–623 (2013).
- ⁹⁰N. Olsman and L. Goentoro, "Allosteric proteins as logarithmic sensors," *Proc. Natl. Acad. Sci.* **113**, E4423–E4430 (2016).
- ⁹¹D. Ben-Avraham and S. Havlin, *Diffusion and Reactions in Fractals and Disordered Systems* (Cambridge University Press, Cambridge, 2000).
- ⁹²D. L. Koch and J. F. Brady, "Anomalous diffusion in heterogeneous porous media," *Phys. Fluids* **31**, 965–973 (1988).
- ⁹³M. Küntz and P. Lavallée, "Experimental evidence and theoretical analysis of anomalous diffusion during water infiltration in porous building materials," *J. Phys. D: Appl. Phys.* **34**, 2547 (2001). <https://iopscience.iop.org/article/10.1088/0022-3727/34/16/322>.
- ⁹⁴A. Grosman and C. Ortega, "Capillary condensation in porous materials. Hysteresis and interaction mechanism without pore blocking/percolation process," *Langmuir* **24**, 10515–10521 (2005).